Z. Phys. D 34, 227–232 (1995)

ZEITSCHRIFT
FÜR PHYSIK D

Doppler free "dark resonances" for hyperfine measurements and isotope shifts in Ca^+ isotopes in a Paul trap

F. Kurth[1], T. Gudjons[1], B. Hilbert[1], T. Reisinger[1], G. Werth[1], A.-M. Mårtensson-Pendrill[2]

[1]Institut für Physik, Universität Mainz, D-55099 Mainz, Germany
[2]Department of Physics, Chalmers University of Technology and Göteborg University, S-412 96 Göteborg, Sweden

Received: 7 June 1995

Abstract. We have observed "dark resonances" in the Λ-type level structure, formed by the $4S_{1/2}$ ground state, the $4P_{1/2}$ excited state and the low lying metastable $3D_{3/2}$ state in the Calcium ion, confined in a Paul radio-frequency trap. These Doppler-free and potentially very narrow resonances were used to determine the magnetic dipole hyperfine interaction constant A for the $4P_{1/2}$ and $3D_{3/2}$ state of $^{43}Ca^+$, giving $-142(8)$ MHz and $-48.3(1.6)$ MHz, respectively. From measurements of the P-D (E1) and S-D (E2) transition wavelength in a mixture of $^{43}Ca^+$ and $^{40}Ca^+$ we determined the isotope shifts of these lines.

PACS: 32.80.P; 31.30.Gs

I. Introduction

"Dark resonances", i.e. the absence of fluorescence from an excited state, appear in a Λ-type level structure (Fig. 1), when two lasers excite simultaneously the transitions from the initial and final state to the common intermediate state for a given velocity class of the atom or ion [1]. If the fluorescence from the intermediate state is monitored, one observes a minimum in the count rate, since the occupation number in this state drops to zero and the intermediate level acts as a mere relay in the coherent superposition, formed by the two lasers between the initial and final state. The linewidth of this "dark resonances" is free of first order Doppler effects and depends ultimately only on the lifetimes of the initial and final state. The Calcium ion has a favourable level structure for such investigations: The ground $4S_{1/2}$ state can be excited by a strong E1 transition to the $4P_{1/2}$ level at 397 nm, a second transition at 866 nm connects the $4P_{1/2}$ state to the $3D_{3/2}$ level also by E1 radiation. The lifetime of the metastable $3D_{3/2}$ state has been determined to 1.113(45) s [2], which gives rise to a natural linewidth below 1 Hz and makes the dark resonance a potential candidate for frequency standard application. In addition to these mentioned levels, the Ca^+ level scheme (Fig. 1) contains a $4P_{3/2}$ and a $3D_{5/2}$ state (τ = 1.054(61) s[2]). The later one gives rise to possibilities for high precision experiments on laser cooled Ca^+ ions, using the quantum amplifier scheme on the weak $4S_{1/2}$–$3D_{5/2}$ or $3D_{3/2}$–$3D_{5/2}$ transition. The particular advantage of Ca^+ arises from the fact that all wavelengths can in principle be produced by small diode laser systems (including frequency doubling). Similar level shemes appear in several ions of the alkaline earths, and dark resonances have been observed previously in Ba^+ [3,4].

II. Experimental setup

The trapped ion technique was used to exploit the long lifetime of the metastable $3D_{3/2}$ state. A cloud of about 10^5 Ca^+ ions, consisting of 20% of ^{40}Ca and 80% of ^{43}Ca, was confined in a Paul trap. We used a Paul quadrupole trap of 20 mm radius, driven by 600 V a.c. amplitude at $\Omega/2\pi$ = 1 MHz and V_{dc} = 10 V (Fig. 2). The ions were buffer gas cooled by $3 \cdot 10^{-6}$ mbar of Helium and the storage time was of the order of 1 day. The UV and IR laser beams at 397 and 866 nm from a frequency doubled Ti:S laser and a diode laser, respectively, entered the trap colinearly through 3 mm apertures in the x-y plane of the ring electrode and the ionic fluorescence at 397 nm was collected perpendicular to the laser beams through a mesh endcap electrode. Using 10 mW power for the UV laser and 5 mW for the IR laser power, the count rate at resonance center was of the order of 1 MHz. The total detection efficiency including solid angles, transmission losses and photocathode efficiency can be estimated to about $3 \cdot 10^{-4}$.

A "dark resonance" in the trapped Ca^+ ions occurs, if the laser detunings from the $4S_{1/2}$–$4P_{1/2}$ and $4P_{1/2}$–$3D_{3/2}$ resonances are chosen in a way that both lasers meet the resonance for the same velocity class of the ions due to their Doppler shift. This Doppler shift arises mainly from the oscillating motion of the ions in the time varying electric trapping field (micromotion). The oscillation causes a frequency modulation of the laser fields in the rest frame of the ions. The modulation frequency (1 MHz) is slow compared to the time scale for optical excitation (10^{-8} s) and the modulation amplitude from the ion motion (typical Doppler width 1 GHz) is large compared to the natural line width. The condition for proper laser detuning in the dark resonance then is

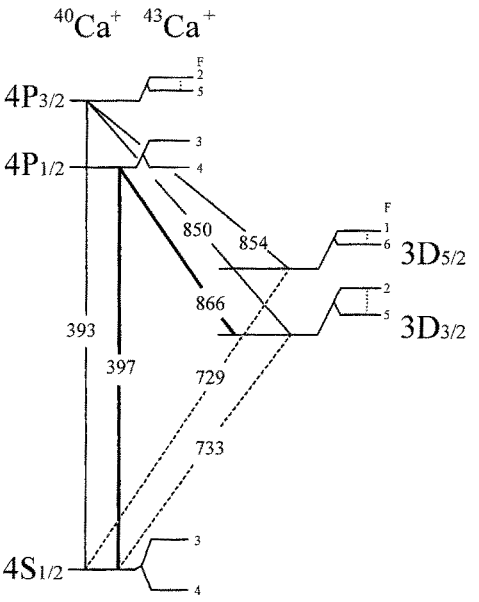

Fig. 1. Partial level sheme of $^{40}Ca^+$ and $^{43}Ca^+$ indicating the hyperfine splitting and isotope shift. The hyperfine constants for the $4S_{1/2}$, $4P_{1/2}$, $4P_{3/2}$, $3D_{3/2}$ and $3D_{5/2}$ level are on the order of -806 MHz, -145 MHz, -30 MHz, -50 MHz, and -5 MHz, respectively [see Table in 1, 5, 6]. The 4S–3D electric quadrupole transitions are characterized by a dashed line. All wavelength given are in nm

$$\Delta_{UV}/\Delta_{IR} = k_{UV}/k_{IR} \tag{1}$$

where Δ_{UV}, Δ_{IR} describes the detunings for UV and IR laser, respectively, and k_{UV}, k_{IR} are the corresponding wave vector amplitudes.

The simple 3-level scheme of $^{40}Ca^+$ exhibits one dark resonance, as evident from Fig. 3. A possible Zeeman splitting in the residual magnetic field in our lab is not resolved. For $^{43}Ca^+$, having a nuclear spin of 7/2 the situation is more complex, as discussed in the next section.

III. Hyperfine structure

The interaction between the magnetic moments of the electrons and the nucleus gives rise to a hyperfine structure of $^{43}Ca^+$, commonly described by an effective interaction $A\mathbf{I}\cdot\mathbf{J}$, which leads to a hyperfine splitting of the S, P and D-states. All combinations of hyperfine levels of the ground and excited states having non-zero matrix elements in the transition probability for the two-photon resonance

$$\langle J_S, F_S|E1|J_P, F_P\rangle\langle J_P, F_P|E1|J_D F_D\rangle \tag{2}$$

can lead to a dark resonance. J_S, F_S ... denotes the J and F quantum numbers of the S-electronic state and analogous for the other levels, E1 is the electric dipole operator. For $^{43}Ca^+$ this leads to a total number of 12 dark resonances. The reduction in count rate for each of these resonances is small due to the large background from the remaining Doppler broadened transitions. Only a part of them can be ovserved for a given laser detuning. Our experimental procedure was to keep the UV laser fixed and scan the IR laser across the 4P–3D resonances. We then changed the UV laser to a different detuning and scanned the IR laser again in order to observe different dark resonances. In this way all possible resonances with non-vanishing dipole matrix elements according to (2) have been detected. In addition we observed resonances at the $4S_{1/2}$ $(F = 4)$ – $4P_{1/2}$ $(F = 4)$ – $3D_{3/2}$ $(F = 2)$ and $4S_{1/2}$ $(F = 3)$ – $4P_{1/2}$ $(F = 3)$ – $3D_{3/2}$ $(F = 5)$ wavelength (Fig. 3) which contain matrix elements of an electric quadrupol transition. We attribute the appearance of that weak transition to a strong population of the $3D_{3/2}$ ($F = 2$ and $F = 5$) states from optical pumping. These optical pumping processes together with the unknown direction of the residual magnetic field in our laboratory and a given polarisation of the laser makes it difficult to predict the strength of each resonance. Whereas the Ti:S UV laser is stabilized to an external cavity, the IR laser uses feedback by a grating and is not actively stabilized. The residual linewidth of the two lasers is of about 1 MHz in the UV and 5 MHz in the IR. In order to reduce frequency shifts and line broadenings from the laser drifts, we scanned the IR laser fast (about 5 MHz/100 ms) across the resonance, repeated the scans and added them to improve the signal/noise ratio. Frequency calibration was performed by a 50 cm confocal marker cavity FSR = 150.3 MHz), which itself was calibrated using EOM sidebands.

The dark resonances become better visible if we subtract a smooth envelope from the signal (Fig. 3). The sum of several of these resonances can be well fitted by a Lorentzian lineshape (Fig. 4).

The $^{43}Ca^+$ spectrum consists of two groups of lines, where the large splitting is due to the hyperfine structure of the $4S_{1/2}$ ground state. The splitting within the groups corresponds to the hyperfine structure of the excited levels. For the interpretation of the spectra, one has to include the information already known. This is mainly the ground state hyperfine splitting, which we measured previously to 3.2256 GHz using a laser microwave double resonance technique [5]. According to (1) this splitting appears in the IR-spectrum as 1.478 GHz, i.e. the two lasers are Doppler-shifted to resonance for ions of the same velocity. We then can assign lines, which correspond to equal 4P and 3D F-quantum numbers. Comparison with a spectrum, calculated with the theoretical predictions for the A-factors allows final identification. The two lines at the extreme ends of the spectrum correspond to the $\Delta F = 2$ transitions.

From the observed dark resonances we calculated the A-factors for the $4P_{1/2}$ and $3D_{3/2}$ level from all combinations of two hyperfine-level distances. Our results are A $(4P_{1/2}) = -142(8)$ MHz and A $(3D_{3/2}) = -48.3(1.6)$ MHz (Table 1), in good agreement with theoretical results obtained using many-body perturbation theory [6, 7]. These calculations include pair correlation to high order, with the later calculation [7] including more pair excitations and more iterations, made possible by the development of workstations. Table 1 also gives a comparison with other available experimental and theoretical data [8–10].

Also the nuclear electric quadrupole moment, Q, affects the hyperfine structure of the states with $j > 1/2$. We included this electric hyperfine structure of the $3D_{3/2}$ level in our analysis and obtained the limits -6.5 MHz $< B < 5.5$ MHz. Theoretical calculations [6] give $B/Q \approx 69$ MHZ/b, which, combined with the tabulated quadrupole moment $Q(^{43}Ca) = -40,8(8)$ mb [11], would give $B \approx -2.8$ MHz.

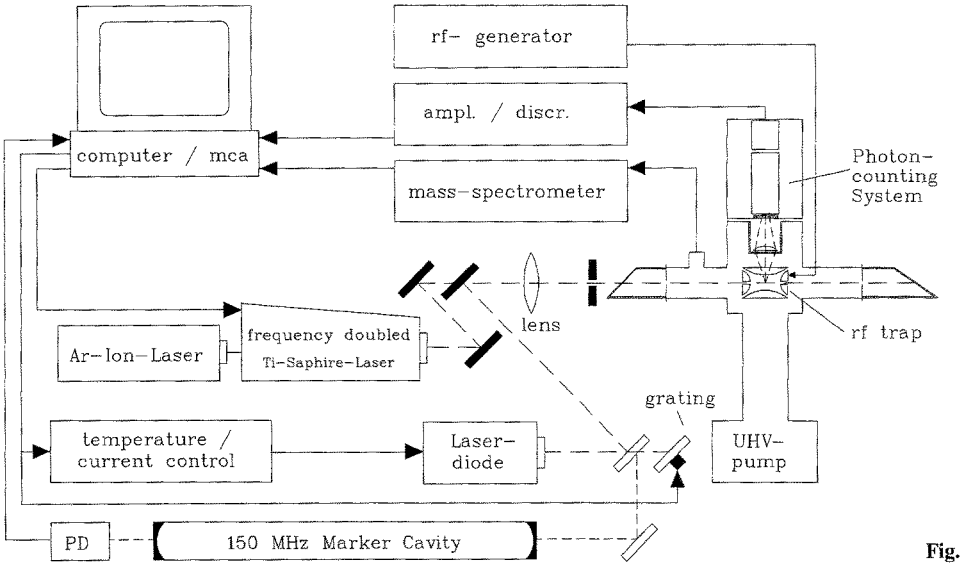

Fig. 2. Experimental setup

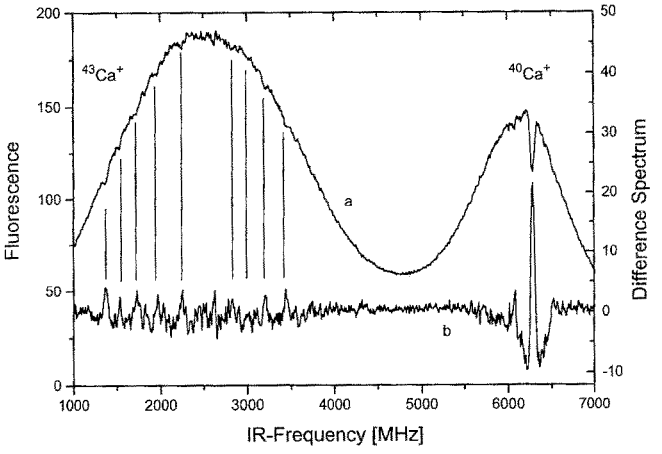

Fig. 3. Laser induced fluorescence from the $4P_{1/2}$ level in a mixture of $^{40}Ca^+$ and $^{43}Ca^+$ showing Doppler broadened resonances at the $4P_{1/2}$–$3D_{3/2}$ transition wavelength and superimposed Doppler free "dark resonances" (*a*). The second laser at the $4S_{1/2}$–$4P_{1/2}$ transition was held at a fixed wavelength. (*b*) Shows the difference of spectrum (*a*) to a smooth envelope for better visibility of the "dark resonances"

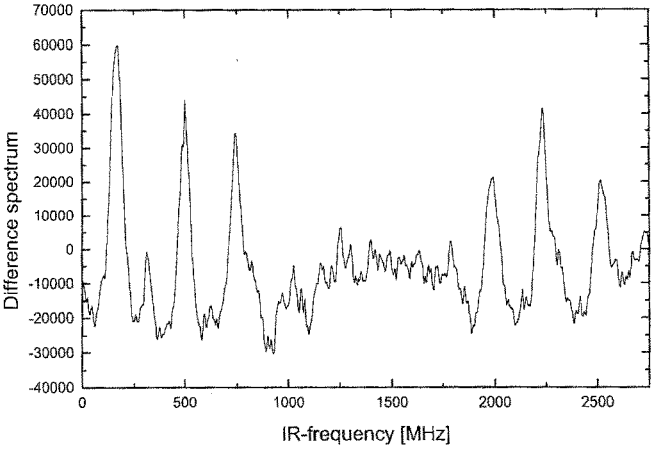

Fig. 4. Sum over several difference spectra showing "dark resonances"

IV. Isotope shifts

The transition energies differ between ^{40}Ca and $^{4}3Ca$, not only because of the non-zero nuclear magnetic moment of ^{43}Ca, but also due to different nuclear masses and charge distribution. These differences lead to an isotope shift of the transition energies. This shift can be written as

$$\delta\nu_i^{A,A'} = K_i^{MS}\frac{M_A - M_{A'}}{(M_A + m_e)M_A} + F_i(1-\kappa)\delta\langle r^2\rangle A, A' \qquad (3)$$

where the first term is the mass shift accounting for the nuclear motion and the second term is the field shift arising from the change in electrostatic potential from the nucleus due to the change in charge distribution.

In the many-body perturbation theory calculations presented in Sect. IV.B, the shifts in the one valence system, Ca^+, are expressed in terms of individual level shifts with respect to the unperturbed closed-shell core, i.e. Ca^{2+}. The shift in a transition is then given as the shift of the lower level minus that of the upper level. The results of several isotope shift measurements for Ca, including various methods and transitions, were combined by Palmer et al. [12] in a multi-dimensional King plot, with the aim of obtaining improved results for the changes in charge distribution. They recommend the value $\delta\langle r^2\rangle^{40,43} = 0.1254(32)\,\mathrm{fm}^2$ for the isotopes considered in this work.

Table 1. Magnetic dipole interaction constants A in $^{43}Ca^+$

State	Experimental results (this work)	Experiments results (other authors)	Theoretical calculations
$4P_{1/2}$	−142(8) MHz	−158(3.3) MHz [8]	−148 MHz [6]
		−145(1.0) MHz [9]	−144 MHz [7]
			−135.7 MHz [10]
$3D_{3/2}$	−48.3(1.6) MHz		−52 MHz [6]
			−49.4 MHz [6]

Table 3. Isotope shifts for various transitions in Ca^+. The RIS values were obtained by subtracting the NMS from the experimental shifts, and the field shift (FS) values were obtained using $\delta\langle r^2\rangle^{40,43} = 0.1254(32)\,fm^2$ [12]

Transition	Wavelength (nm)	IS (MHz)	RIS (MHz)	FS (MHz)	K^{SMS}(exp) (GHz u)
$3D_{3/2} \rightarrow 4P_{1/2}$	866.45	−3483(40)	−3814(40)	11	−2191(23)
$3D_{3/2} \rightarrow 4P_{3/2}$	850.04	−3446(20)	−3784(20)	11	−2173(11)
$3D_{5/2} \rightarrow 4P_{3/2}$	854.44	−3427(33)	−3763(33)	11	−2161(19)
$4S_{1/2} \rightarrow 3D_{3/2}$	732.59	4180(48)	3788(48)	−47	2196(28)
$4S_{1/2} \rightarrow 3D_{5/2}$	729.35	4129(18)	3735(18)	−47	2166(10)
$4S_{1/2} \rightarrow 4P_{1/2}$	396.96	706(42)	−17(42)	−35	10(24)
		672(9) [7]	−51(9)	−35	−9(5)
		685(36) [14]	−38(36)	−35	−2(21)
$4S_{1/2} \rightarrow 4P_{3/2}$	393.48	713(31)	−17(31)	−35	10(18)
		677(19) [7]	−53(19)	−35	−10(11)
		685(36) [14]	−45(36)	−35	−5(21)

A. Experimental determination of isotope shifts

We determinated the isotope shift of the allowed P-D transitions. We obtained for the different transitions in $^{43}Ca^+$ and $^{40}Ca^+$ the following shifts

$3D_{3/2}$–$4P_{1/2}$ (866 nm): −3483(40) MHz
$3D_{3/2}$–$4P_{3/2}$ (850 nm): −3446(20) MHz
$3D_{5/2}$–$4P_{3/2}$ (854 nm): −3427(33) MHz .

Motivated by these rather large isotope shifts, we complemented the measurements by investigation of the electric quadrupole lines, connecting the $4S_{1/2}$ ground state with the 3D-levels. For this experiment we used the Ti:S laser at 729 nm or 733 nm to obtain sufficient power to drive the weak E2 transition. Another marker cavity with a FSR of 228.8 MHz served for scan calibration. We probed the D-state population by a laser diode exciting the corresponding D–P transition. We then overserved the fluorescence from the P-state into the ground level free of any laser straylight. Since the S–D resonance is forbidden in first order and Doppler broadened, we had to use full available laser power ($\approx$ 500 mW) and to scan the laser very slowly (25 MHz/s) across the resonance. To avoid optical pumping between the hyperfine levels of $^{43}Ca^+$ we irradiated the ions simultaneously by the ground state hyperfine splitting frequency of 3.2 GHz. In the observed spectra one can clearly resolve the ground state hyperfine splitting (Fig. 5) while the $3D_{3/2}$ splitting is obscured by the Doppler broadening of the lines. Comparison with a simulated S-D line shape was used to calculate the center of mass of this double peak. The $^{40}Ca^+$–$^{43}Ca^+$ isotope shift of this line has been determined to

$4S_{1/2}$–$3D_{3/2}$ (733 nm): 4145(43) MHz
$4S_{1/2}$–$3D_{5/2}$ (729 nm): 4129(18) MHz .

The calculations presented below show that these large shifts are mainly due to the specific mass shift (SMS) of the 3D state.

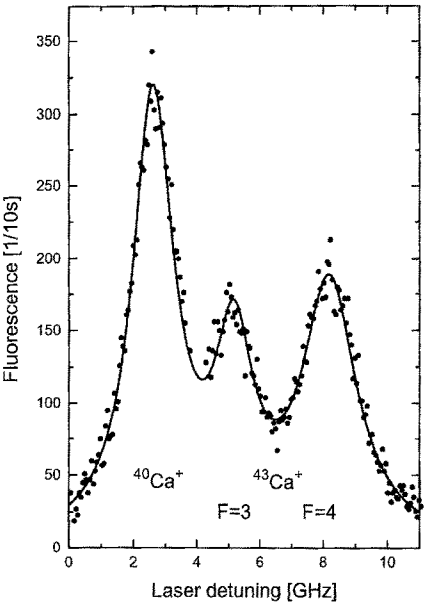

Fig. 5. Laser induced electric quadrupole transition $4S_{1/2}$–$3D_{3/2}$ in a mixture of $^{40}Ca^+$ and $^{43}Ca^+$. The ground state hyperfine splitting in $^{43}Ca^+$ is well resolved, while the $3D_{3/2}$ splitting is smaller than the Doppler width

Table 2. Calculated contributions to the mass shift constant K^{SMS}_{3Dj}, for the $3D_{3/2}$ and $3D_{5/2}$ orbitals in units of GHz u. The values are expected to be increased by the modification of the valence orbital to approximate Brueckner orbitals, as discussed in Sect. IV.C. The mass shift constants $K^{SMS}_{4S} = -237$ GHz u and $K^{SMS}_{4P} = -218$ GHz u were obtained in earlier work [24]

	$3D_{3/2}$ (GHz u)	$3D_{5/2}$ (GHz u)
DF	−4313	−4298
RPA	1838	1827
Corr, cv	1844	1838
Corr, cc	−982	−980
Total:	−1613	−1612

B. The field isotope shift

Differences in the nuclear charge distribution give rise to shifts in the energy levels, $\delta\nu^{FS} = F(1-\kappa)\delta\langle r^2\rangle$, contributing to the total shift given in (3). The electronic factor F for the field shift is given by

$$F = -\frac{4\pi}{6}\Delta|\psi(0)|^2\frac{Ze^2}{4\pi\varepsilon_0} \quad (4)$$

and is determined by the change in electron density, $|\Psi(0)|^2$, at the nucleus between the lower and upper state of the transition. In the non-relativisic limit, only S-electrons contribute directly, but electrons with $l > 0$ can perturb the S electrons in the core, thereby affecting the field shift. In the relativistic formulation, also $P_{1/2}$ electrons have a non-zero wavefunction at the nucleus, but their contribution is negligible for low Z, where relativistic effects can essentially be accounted for by application of the relativistic correction factor appropriate for S electrons, found to be 1.18 for Ca. Multiplying the non-relativistic coupled-cluster results by this correction led to the electronic factors [13]

$$F_{4S} \approx -261\,\mathrm{MHz/fm^2}$$

$$F_{4P} \approx +21.8\,\mathrm{MHz/fm^2}$$

$$F_{3D} \approx +110\,\mathrm{MHz/fm^2}\ .$$

The negative F factor for the 4S state is dominated by the contribution from the valence electron itself, whereas the positive F factors for the 4P and 3D states reflect a reduced core electron density at the nucleus caused by the presence of the valence electron.

The correction term, κ in (3) accounts for higher moments, $\delta\langle r^4\rangle$, $\delta\langle r^6\rangle\ldots$, of the nuclear charge distribution, but is negligibly small (about 0.4%) for Ca.

The field shifts for the relevant levels are thus obtained as $\delta\nu^{\mathrm{FS}}_{4S} = -32.7\,\mathrm{MHz}$, $\delta\nu^{\mathrm{FS}}_{4P} = 2.7\,\mathrm{MHz}$ and $\delta\nu^{\mathrm{FS}}_{3D} = 13.8\,\mathrm{MHz}$, giving the transition field shifts shown in Table 3. We see that the changes in the nuclear charge distribution account for only a small part of the total isotope shift.

C. The mass isotope shift

The mass shift can be divided into two terms in the non-relativistic limit, characterized by the factor $K^{\mathrm{MS}} = K^{\mathrm{NMS}} + K^{\mathrm{SMS}}$. The first part, $K^{\mathrm{NMS}} = m_e\nu$, gives the "normal mass shift", which accounts for the effect of substituting the electron mass, $m_e = 5.4858\cdot 10^{-4}$u by the reduced mass $\mu = m_eM/(m_e + M)$ in the Schrödinger equation. The second part, $K^{\mathrm{SMS}} = \Delta(\Sigma_{i>j}P_i\cdot P_j)/h$, involves two electrons simultaneously and describes a correlation between the electronic momenta arising through the motion of the nucleus. The mass shift between the two Ca isotopes is obtained by multiplication of the mass shift factor, K^{MS}, with the mass factor

$$(M_{43} - M_{40})/(M_{40}(M_{43} + m_e)) \approx 0.001746/\mathrm{u}\ . \quad (5)$$

The nuclear masses $M_{40} = 39.951618$u and $M_{43} = 42.947795$u are obtained by subtracting $20\,m_e$ from the atomic masses. Subtracting the normal mass shift from the experimental isotope shift leads to the *residual isotope shift*, RIS.

The leading contributions to the SMS constant for the 4S, 4P and 3D states of Ca^+ have been calculated within the framework of many-body perturbation theory, using a numerical relativistic basis set [15] obtained in the Dirac-Fock (DF) potential from the closed shell Ca^{2+} ion. In this way, the shift of each level with respect to the Ca^{2+} ion is obtained directly, without the need to subtract and cancel out enormous contributions from an unperturbed closed shell core. By using relativistic orbitals, some, but not all of the relativistic corrections [16, 17] to the mass isotope shift are included, as discussed e.g. by Drake [18]. A relativistic modification of the SMS operator is given by Shabaev [19], but has not yet been implemented in our computer programs.

The calculations presented here follow the procedure described in earlier work for Cs and Tl [20], and which has been applied also to Yb^{2+} [21] and Ba^{2+} [13] and to the shift in the electron affinity of Cl [22].

Table 2 shows the contributions obtained for the 3D states, which are found to be essentially independent of the j value, indicating that the problem is mainly nonrelativistic. The largest individual term -4.3 THz u arise from the term $\Sigma\langle vc|\mathbf{p}_1\cdot\mathbf{p}_2|cv\rangle$, involving the valence electron, v, and all core electrons c of opposite parity. The inner core orbitals, with their larger momenta, dominate this term. The nuclear motion affects the waveform of all electrons, thereby modifying, e.g. the interaction between the core and the valence electron. The change in the binding energy due to the first-order correction of the core cancels a large part of the DF contribution, leaving a sum of only -2.5 THz u. We note that Bauche [23], in his pioneering non-relativistic isotope shift calculations, performed seperate Hartree- Fock calculations for the initial and final states and in this way include automatically also the 'RPA' terms. Being a two particle operator the SMS is very sensitive to correlation effects, which arise already in second order. For the 3D states, these bring the final result down to -1.6 THz u. Analogous calculations were performed for the 4S and 4P states, with deviations at the percent level from the non-relativistic values, -198 GHZ u and -167 GHZ u, respectively, given in [24]. From the work on hyperfine structure [6], we know that correlation effects lead to a contraction of the valence orbital, made possible by the core adjusting to the presence of the valence electron. The effect on the valence orbital gives an increase in the valence electron expectation value of the hyperfine structure for the 4S, 4P and 3D states by about 18%, 20%, and 34% , respectively [6]. Also the SMS is dominated by the region close to the nucleus, since the momenta are higher here. The contraction can the be expected to give an increase also for the SMS, of roughly the same order, as confirmed by the non-relativistic calculations for the 4S and 4P orbitals [24], where the inclusion of the first-order Brueckner orbital correction resulted in $K^{\mathrm{SMS}}_{4S} = -237$ GHz u and $K^{\mathrm{SMS}}_{4P} = -218$ GHz u. Assuming the SMS constant for the 3D state increases by about the same amount as the HFS would lead to an estimate for K^{SMS}_{3D} of approximately -2.1 THz u.

D. Comparison between theoretical and experimental results

Table 3 shows experimental transition shifts (IS) together with the residual isotope shifts (RIS), obatined by removing the reduced-mass effect. The fifth column gives the field shift (FS), evaluated as discussed in Sect. IV.B. We see that the field shift is essentially negligible for the transitions involving a 3D state, in agreement with the calculations, which gave very large values for the SMS for the 3D states.

By contrast, the isotope shift of the 4S-4P transition is dominated by the NMS. The SMS is very small, although this small numbers arise from a cancellation between the much larger SMS values of the individual 4S and 4P states.

Subtraction of the field shift from the RIS, and dividing the result by the mass factor in (5), allows an experimental estimate of the SMS constant, leading to $K_{3D}^{SMS} \approx -2.4\,\mathrm{THz}$ u. This result is about 50% larger than the lowest-order results, given in Table 2. As discussed in Sect. IV.C., an increase of this order can be expected from the modification of the orbitals to approximate Brueckner orbitals, giving a value of about $-2.1\,\mathrm{THz}$ u. However also other types of correlation effects are expected to be important for 3D electrons.

V. Discussion

This paper demonstrates the wide field of possible applications of Paul traps in modern spectroscopy. Using the nonlinear effect of dark-resonances it was for the first time possible to obtain an experimental result for the hyperfine structure of the $3D_{3/2}$ level in $^{43}Ca^{+}$. Furthermore earlier measurements of the $4P_{1/2}$ hyperfine structure constant could be confirmed. It should be pointed out that the used methode has not reached its limits yet, since this experiment is at present time limited by the line width and the jitter of the lasers. Furthermore may the use of modulation techniques allow to reduce the needed laser power and such reduce the power broadening. Good agreement is obtained between theoretical and experimental results, also for the strongly correlated 3D state.

The second part of this work focussed on the isotope shifts in $^{43}Ca^{+}$ vs. $^{40}Ca^{+}$. Besides the prior observed shift on the 4S–4P lines we could present measurements of all 4S–3D and 3D–4P lines. These show an unusual large shift of about 4.1 GHz and $-3.4\,\mathrm{GHz}$ repectively. Although higher-order effects would have to be included also for the mass shift in order to get reliable results, already the limited calculation presented here accounts qualitatively for the large isotope shifts observed in transitions involving the 3D states.

Financial support from the Deutsche Forschungsgemeinschaft and from the Swedish Natural Science Research Council is gratefully acknowledged.

References

1. Alzetta, G., Gozzini, A., Moi, L., Orriols, G.: Nuovo Cimento B **36**, 5 (1976)
2. Arbes, F., Benzing, M., Gudjons, T., Kurth, F., Werth, G.: Z. Phys. D **29**, 159 (1994)
3. Janik, G., Nagourney, W., Dehmelt, H.: J. Opt. Soc. Am B **2**, 1251 (1985)
4. Siemers, I., Schubert, M., Blatt, R., Neuhauser, W., Toschek, P.E.: Europhys. Lett. **18**, 139 (1992)
5. Arbes, F., Benzing, M., Gudjons, T., Kurth, F., Werth, G.: Z. Phys. D **31**, 27 (1994)
6. Mårtensson-Pendrill, A.-M., Salomonson, S.: Phys. Rev. A **30**, 712 (1984)
7. Mårtensson-Pendrill, A.-M., et al.: Phys. Rev. A **45**, 4675 (1992)
8. Goble, A.T., Maleki, S.: Phys.Rev. A **42**, 1 (1990)
9. Silverans, R.E., et al.: Z. Rev. D **18**, 351 (1991)
10. Meulebeke, G.V.: Contribution à létude théorique des effects de la corrélation électronique en spetroscopie atomique. Université Libre de Bruxelles, Faculté des Sciences, and M. Godefroid (private communication)
11. Pyykö, P., Li, J.: J. Chem. Phys. **98**, 7152 (1993)
12. Palmer, C.W.F., et al.: J. Phys. B **17**, 2197 (1984)
13. Villemoes, P., Arnesen, A., Heijkenskjöld, F., Wännström, A.: J. Phys. B **26**, 4289 (1994)
14. Maleki, S., Goble, A.T.: Phys. Rev. A **45**, 524 (1992)
15. Salomonson, S., Öster, P.: Phys. Rev. A **40**, 5548 (1989)
16. Stone, A.P.: Proc. Phys. Soc. London **77**, 786 (1961)
17. Stone, A.P.: Proc. Phys. Soc. London **81**, 868 (1963)
18. Drake, G.W.F.: In: Long-range Casimir forces: theory and recent experiments on atomic systems. Levin, F.S., Micha, D.A. (eds.) pp. 107–217. New York: Plenum 1993
19. Shabaev, V.M., Artemeyer, A.N.: J. Phys. B **27**, 1307 (1994)
20. Hartley, A., Mårtensson-Pendrill, A.-M.: J. Phys. B **24**, 1193 (1991)
21. Mårtensson-Pendrill, A.-M., Gough, D.S., Hannaford, P.: Phys. Rev. A **49**, 3351 (1994)
22. Berzinsh, U., et al.: Phys. Rev. A **51**, 231 (1995)
23. Bauche, J.: J. Phys. (Paris) **35**, 19 (1974)
24. Lindroth, E., Mårtensson-Pendrill A.-M., Salomonson, S.: Phys. Rev. A **31**, 58 (1985)